http://dx.doi.org/10.21577/0103-5053.20190129

J. Braz. Chem. Soc., Vol. 31, No. 1, 201-210, 2020
Printed in Brazil - ©2020 Sociedade Brasileira de Química

Short Report

TiO_2 Decorated Sand Grains for Photodegradation of Pollutants: Methylene Blue and Ciprofloxacin Study

Jorge A. S. Lacerda,[a] Allan M. Macedo,[b] Rodolfo I. Teixeira,[b] Grazieli Simões,[b] Emerson S. Ribeiro,[b,c] Josué S. B. Forero[b] and Rodrigo J. Corrêa[*,b,c]

[a]*Centro de Pesquisas e Desenvolvimento Leopoldo Américo Miguez de Mello (CENPES), Petróleo Brasileiro S.A. (PETROBRAS), 21941-915 Rio de Janeiro-RJ, Brazil*

[b]*Instituto de Química, Universidade Federal do Rio de Janeiro (UFRJ), 21941-909 Rio de Janeiro-RJ, Brazil*

[c]*Instituto Nacional de Tecnologias Alternativas para Detecção, Avaliação Toxicológica e Remoção de Micropoluentes e Radioativos (INCT-DATREM), Instituto de Química, Universidade Estadual Paulista (Unesp), CP 355, 14800-900 Araraquara-SP*

This study shows a preparation and evaluation of a new non-expensive TiO_2 based photocatalyst built over sand grains surfaces as an alternative green technology for water treatment. The semiconductor covalently bonded to the silica sand grains (sand@TiO_2) prepared by hydrolysis of isopropoxide orthotitane over sand grains, showed a high surface area 296 $m^2\ g^{-1}$ and a high reaction rate for methylene blue (MB) photodegradation (0.064 min^{-1}), on steady state condition by using 3 g of sand@TiO_2 and an MB solution (20 mL, 3×10^{-5} mol L^{-1}) or ciprofloxacin hydrochloride (CIP) solution (20 mL, 1.9×10^{-3} mol L^{-1}). Under UV irradiation with a medium pressure Hg lamp, the total MB removal reached 70% after 7 min and 45% for CIP in 60 min. Further, the photocatalyst showed to be a promising reusable material for removal of ciprofloxacin hydrochloride antibiotic (CIP) on wastewater. This new material appears as a new promising low cost and low impact reusable catalyst for water treatment.

Keywords: TiO_2, methylene blue, ciprofloxacin, photodegradation, reusable catalyst

Introduction

The development of greener technologies for the near future is believed to involve catalysis, agreeing with the twelve principles of green chemistry.[1] In fact, the scientific community has already turned its attention to apply Green Chemistry parameters according to life cycle assessment (LCA) methodology to evaluate the chemical processes related to catalysts like TiO_2 arising as one of the best choice catalysts for environmental purposes.[2-4] Dyes decomposition from textile wastewater (like methylene blue, MB) is recognized as an important environmental treatment due to their potential toxicity and coloration.[5] Additionally, life has changed dramatically in the last century and all human way of living is deeply dependent upon antibiotics from fluoroquinolone family, such as ciprofloxacin hydrochloride (CIP) (Scheme 1). These drugs show a large usage spectrum, but they are mainly employed in the treatment of urinary tract infection and prostatitis. They have also been used against bacterial infections such as enteric and biliary tract ones, as well as treating sexually transmitted diseases, and in the prophylaxis of immunocompromised neutropenic host. It is worthwhile to emphasize here that CIP is the most used antibiotic in the world and a direct consequence of such scenario is the forced selection of resistant strains and a profound impact on ecosystems balance and human health due to the antibiotic resistance increase (AR).[6-8]

Around 40 to 50% of CIP can leave the target organisms unaltered, meaning that there is a non-metabolized form being excreted to the environment.[7] This antibiotic has been detected in a variety of natural environments, being able to persist for three months until total elimination from river water as showed by Turiel *et al.*[6] Meanwhile, this synthetic

*e-mail: rodrigojosecorrea@gmail.com

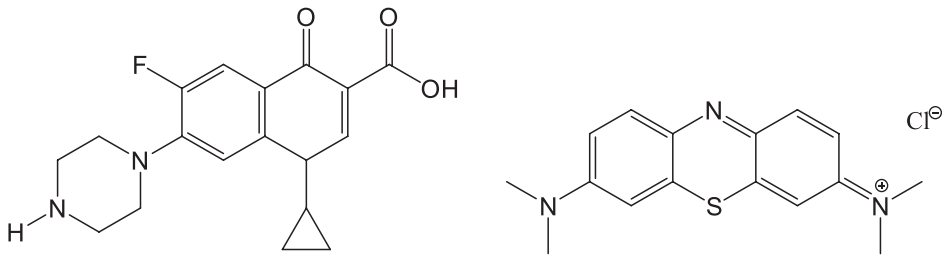

CIP MB

Scheme 1. Chemical structure of CIP antibiotic and methylene blue dye.

drug in sub-inhibitory concentrations can trigger specific transcriptional responses in bacteria,[9-11] so the presence of ciprofloxacin (or antibiotics in general) can dramatically modify the metabolic activity of the microbiota present in polluted areas. Consequently, the environment has been contaminated by these chemicals, including water sources because of its high chemical stability.

Therefore, a fast-increasing demand for potable water has promoted the development of different purification alternatives methods like adsorption, ozonation, chlorination, UV and photocatalysis.[12] Among all these alternatives, the use of semiconductor photocatalysts are the greener approach in terms of energetic demand, versatility, low-cost and, furthermore, it also emerges as a possible solar based methodology for pollutants degradation,[13-16] in addition to the methodologies using UV irradiation.[17,18]

Heterogeneous photocatalysis are a promising technology to minimize human activities associated damage,[19-42] including antibiotics released on wastewaters. Nevertheless, one of its main obstacles has to do with the fact that the catalysts (TiO_2, for instance) are non-soluble thin solid particles, turning aqueous solutions turbid, thus reducing light flux into the reaction medium. So, unfortunately, despite the substantial number of scientific studies on photocatalysis of environmental impacting compounds there is still a lack of real applications for TiO_2 as everyday photocatalysis. An alternative to overcome this problem can be accomplished by chemically bonding the active photocatalyst to an inert non-soluble matrix, maximizing light absorption due to its high surface area, with a minimum catalyst demand. Earlier results employing TiO_2 deposited over sand grains showed it as a promising photocatalyst for chemicals degradation but the TiO_2 layer was not chemically bonded to the sand grain and thus the material durability was not guaranteed.[43]

Thereby, given our interest in photoactive materials for pollutants degradation on wastewater,[44] it is proposed here an innovative approach to achieve non-expensive and green photocatalysis with active TiO_2 chemically bonded to controlled size sand grains. The material was evaluated in steady state and flow reaction conditions under UV irradiation, using methylene blue as photodegradation probe and tested with ciprofloxacin antibiotic as a way of reducing environmental accumulation by inappropriate disposal.

Experimental

TiO_2 chemically bonded sand (sand@TiO_2) catalyst synthesis

Sand was selected as TiO_2 support due to its low-cost and common use in filters for water treatment. Before the photocalyst coating, the sand grains (200 g) with 150 μm average size were treated with concentrated HCl 37% (125 mL) followed by concentrated HNO_3 (125 mL) and distilled water washing. After drying at 300 °C in a muffle furnace, tetraethyl orthosilicate (TEOS) was added to the solid samples (62.5 mL *per* 100 g of sand), and the mixture was stirred for 2 h, followed by distilled water washing. Titanium isopropoxide (1:1 in CH_2Cl_2), 10 mL, was then added with posterior 10 mL 0.1 mol L^{-1} HCl addition and the solution was stirred for 12 h. The organic solvent was then evaporated by mild heating, followed by distilled water washing and annealing at 500 °C for 6 h.

Catalyst physicochemical characterization

Sample morphology was characterized by field emission scanning electron microscopy/energy dispersive X-ray spectroscopy (FESEM/EDS) in a QUANTA FEG 450 microscope. The determination of the surface area, using the BET (Brauner-Emmett-Teller) multipoint method, and pore volume, using the BJH (Barrett-Joyner-Halenda) method, were performed on a Micromeritics Instrument Corporation Tristar 3000 V6.07. The termogravimetry analysis (TGA) was carried out in a TA Instruments SDT Q600 V20.9 analyzer. Catalysts composition were obtained by X-ray diffractometry (XRD) in a Panalytical EXPERT PRO using Cu tube and X-ray fluorescence

(XRF) in a Panalytical MAGICX PRO using Rh tube. For X-ray photoelectron spectroscopy (XPS) analysis, samples (before and after modification) were deposited on a carbon sticky paper in order to avoid surface charging during the XPS experiment. An uniform layer of the samples were placed in an ultrahigh vacuum chamber (10^{-8} mbar). The equipment used to perform X-ray photoelectron analysis was a UHV Xi ESCALAB 250 spectrometer equipped with a hemispherical electron energy analyzer. The XPS spectra were collected using monochromatic AlKα X-ray source (incident energy = 1486.6 eV) and an electron emission angle of 90° with the surface. Survey scans were recorded with 1 eV step and 100 eV analyzer pass energy and the high-resolution regions with 0.1 eV step and 25 eV analyzer pass energy. The linearity of the energy scale was checked using Cu $2p_{3/2}$ (932.7 eV), Ag $3d_{5/2}$ (368.3 eV) and Au $4f_{7/2}$ (84.0 eV).

Data treatment was performed using the Avantage software (Thermo Fisher) and the C–H signal was used as a reference peak at 284.8 eV binding energy. Peak fitting was carried out with Lorentzian/Gaussian ratio of 30%/70%.

Methylene blue degradation kinetics

The photocatalytic activity of the sand@TiO_2 material was evaluated by measuring the degradation kinetics of methylene blue (MB) in water (pH = 5.5). This dye has been chosen as standard material due to a high molar extinction coefficient, efficient adsorption on oxides surface and a high persistence under UV light exposure. The experiments were carried out on 100 mL pyrex beakers filled with 3 g of sand@TiO_2 submerged in 20 mL solution of MB at 3×10^{-5} mol L^{-1}. Prior irradiation, the reaction medium was kept in dark conditions for 30 min and samples were taken and analyzed periodically until adsorption was completed (no change on solution absorbance). Then, samples were irradiated with 16 × 8 W low-pressure Hg discharge lamps (Sankyo-Denki, G8T5E) for 7 min at 278 K (Scheme S1, Supplementary Information (SI) section). The MB concentration was measured every minute during the 7 min reaction course tracking the 664 nm absorption band, using a Shimadzu UV-2450. In order to obey the Lambert-Beer law all samples were studied using MB absorbances below 1, characterizing solutions where the fraction of absorbed light was less than 90% ($f = (1 - 10^{-A})$, where f is the fraction of absorbed light and A is the absorbance) and, thus, avoiding secondary effects on absorbance. In order to check the catalytic behavior of the new material a new fresh MB solution was added to the used catalyst (not recovered) and the photodegradation was still active having been repeated twice.

Catalyst regeneration tests

The catalyst regeneration capabilities were evaluated with a two-step procedure and evaluated as follows: (*i*) 8 mL of a 10 mg L^{-1} (3×10^{-5} mol L^{-1}) MB solution was added to 3 g of the catalyst and exposed to 11 W, 254 nm UV Phillips lamp throughout 30 min. Dye concentration was tracked by the 664 nm absorption band; (*ii*) after this reaction period the dye solution was discarded, and 8 mL of distilled water was added. Then, the catalyst was further irradiated by 30 min period. The catalyst was submitted to steps 1 and 2 for 3 times and the MB degradation tracked by the 664 nm absorption band.

Flow reactor treatment tests

A commercial UV water disinfection GERMETEC 6PJ-643-1 model (28 W, 0.19 A, 220 V, 60 Hz) reactor was used to evaluate dye degradation by filling the reactor's annular space with 400 g of sand@TiO_2 catalyst (Scheme S2, SI section). The sand was kept inside the reactor by adapting metallic sieves as stoppers at the both ends of the reactor. A 10 mg L^{-1} MB solution was pumped through the reactor under UV light irradiation in a 110 mL min^{-1} flow, in single pass, and recirculating conditions (3 treatment cycles). Samples were collected upstream, as well as downstream and taken to UV-Vis spectrophotometry.

Ciprofloxacin degradation kinetics

The photodegradation of ciprofloxacin hydrochloride antibiotic (CIP) over sand@TiO_2 was followed by measuring the antibiotic absorption band at 276 nm. The experiments were carried out on 100 mL pyrex reactors filled with 3 g of the respective catalyst and 20 mL solution (3×10^{-5} mol L^{-1}). Prior irradiation, the reaction medium was kept in dark conditions for 30 min. The samples were irradiated with 11 W, 254 nm UV Phillips lamp throughout 120 min.

Real wastewater

A real wastewater from a cloth dyeing industry was collected prior the use of any treatment method by the company. The dissolved organic matter concentration was 1.041 g L^{-1} and the most common components are blue dyes (not informed) dissolved in water with pH value at 6.5. Due to the high absorbance in the UV-Vis range, before use the sample was diluted in distilled water until absorbance 0.6 at the maximum (250 nm). The photodegradation of the dyes

in wastewater over sand@TiO_2 was followed by measuring the absorption band at 664 nm. The experiments were carried out on 100 mL pyrex reactors filled with 3 g of the respective catalyst and 20 mL solution. Prior irradiation, the reaction medium was kept in dark conditions for 30 min. The samples were irradiated with 16 × 8 W low-pressure Hg discharge lamps (Sankyo-Denki, G8T5E) for 24 h.

Results and Discussion

Surface morphology of the sand grains was analyzed by FESEM. Figure 1 shows (a) water washed sand grains, (b) sand grains after acid treatment (HCl + HNO_3), (c) sand grains after TEOS reaction and (d) sand@TiO_2 FESEM images. Despite the wide morphologic diversity between grains, it is possible to observe (Figure 1) that the entire coating procedure shows no destruction of the sand grains. However, after modification with supported TiO_2 (Figure 1d), the surface of the sand grain becomes rougher, indicating that the modification (as Scheme 2) was efficient. Also, the presence of roughness on the surface of sand grains provides an increase on the surface area.

By analyzing the FESEM images for TiO_2 supported sand grain at 4.000× magnification (Figure S1, SI section), it is observed that plaques or dense layer are deposited on the surface of the sand grain. Such plaques are probably produced over the formation of a mixed oxide SiO_2/TiO_2, formed on the surface of the sand grain. Also, the analyzed

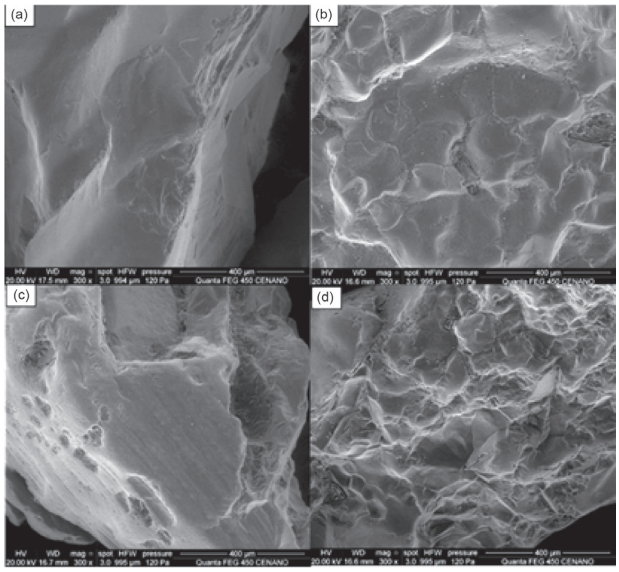

Figure 1. (a) Water washed sand; (b) after acid treatment sand; (c) after TEOS reaction and (d) sand@TiO_2 supported catalyst FESEM images. All magnifications are 300×.

plaque is extremely porous, as can be seen in the magnification of 200,000×. This is an interesting achievement because the high porosity increases the number of active sites on the surface, increasing the photocatalyst efficiency.

FESEM images and the EDS results were obtained in three regions (Figure S2, SI section). The Ti content measured by EDS was 20.2% weight for point 01;

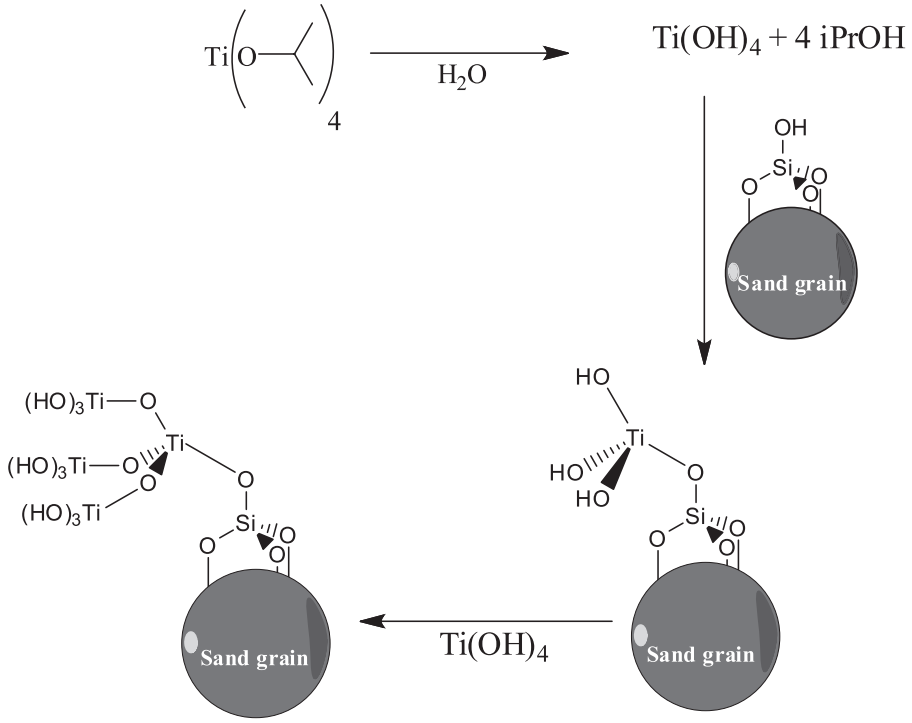

Scheme 2. TiO_2 formation over sand grains.

18.3% weight for point 02 and 1.5% weight for point 03. The values for Ti concentration at points 1 and 2 are close, showing that Ti and Si are highly homogeneous and dispersed due to the formation of the mixed oxide SiO_2/TiO_2, formed on the surface of the sand grain. However, for point 03, the low value of Ti indicates a non-homogeneous coating and surface irregularities, possibly caused by the synthetic procedure in which the sand grains have been submitted to vigorous stirring during the synthesis.

Chemical composition of the sand and sand@TiO_2 samples were analyzed by XPS technique. Survey XPS spectra of the samples are shown in Figure 2 and high-resolution spectra can be found in SI section (Figures S3-S5). As expected, the sand@TiO_2 spectrum exhibit a Ti peak (around 460 eV) in the survey spectra, which is absent in the sand spectrum. The deconvoluted Si 2p XPS spectra of sand@TiO_2 sample show two peaks corresponding to Si–O–Ti and SiO_2, centered at 105.8 and 103.7 eV, respectively. The Ti 2p spectra show the characteristic doublet peak corresponding to split spin-orbit components ($\Delta = 5.8$ eV) involving satellite features. The high resolution O 1s XPS spectra present 3 components: Si–O–Si, Ti–O–Si and Ti–O–Ti with binding energies centered at 534.8, 532.8 and 530.2 eV, respectively.

It is worthwhile to notice that, as mentioned in the "Catalyst physicochemical characterization" sub-section, the TiO_2 layer was assembled over a SiO_2 layer already synthesized over the sand surface, so the EDS results indicate a homogenous TiO_2 layer and the photocatalyst is polydispersed over the sand grain.

XRD analysis was not able to identify anatase or rutile phases on the synthesized catalyst. However, XRF results show the Ti presence (Table 1) confirming the synthetic procedure effectiveness. The Ti concentration determined by XRF is lower if compared by EDS once XRF technique allows a deeper sample penetration (between 1 and 100 μm). So, the XRF technique indicates larger Si

Table 1. XRF results for the presence of different metals on studied sands

	Water washed sand / % mass content	Sand after acid treatment / % mass content	Sand supported TiO_2 catalyst / % mass content
Si	44	44	44
Al	1.9	1.8	1.4
K	1.6	1.7	1.5
Na	0.22	0.26	0.20
Fe	0.10	0.03	0.04
Ca	0.05	0.03	0.05
Ti	0.02	0.02	0.11

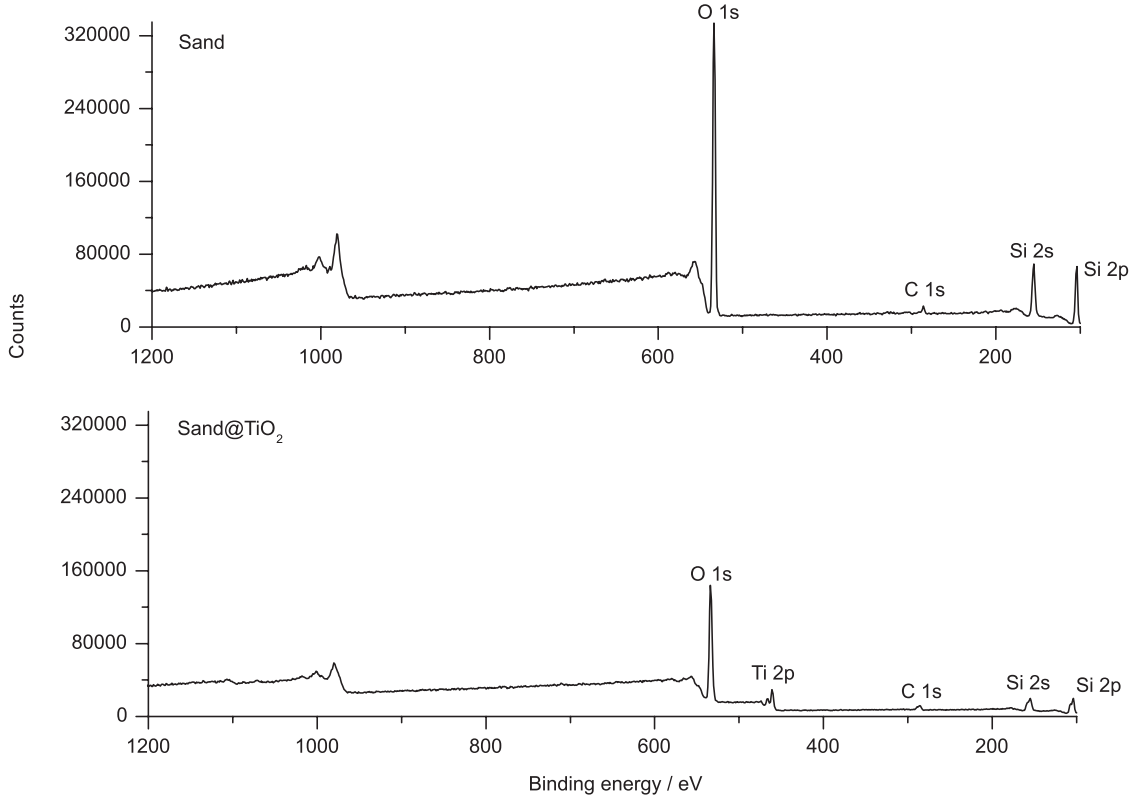

Figure 2. XPS survey spectra of sand grain and sand@TiO_2 samples.

concentration as the bulk of the sand grain being composed by SiO_2 and lower Ti concentration for sand supported TiO_2 catalyst. On the contrary, the EDS technique only scans the surface composition of the sand supported TiO_2 catalyst, and thus, the results show a larger Ti concentration on the catalyst active sites.

Evonik's Aerolyst 7711 catalyst is a TiO_2 bulk solid (100% in mass),[45] while in the sand supported catalyst the TiO_2 effectively responsible for oxidative degradation is a coating, and thus its TiO_2 content is considerably smaller when compared to the Aerolyst 7711. In fact, XRF shows only 0.11% Ti mass content in the sand grains. The theoretical Ti percentage in Aerolyst 7711 is ca. 60% in mass thus the Ti amount on the sand grains is almost 550 times lower than in Aerolyst 7711.

Specific surface area and pore volume obtained by BET technique are shown in Table 2. The sand@TiO_2 catalyst shows the highest surface area and pore volume close to the Aerolyst 7711, although inferior (ca. 28 times lesser). If one considers that a typical catalyst like Y zeolite has a pore volume in the range of 0.20 cm^3 and surface area close to 600 $m^2\ g^{-1}$,[44] TiO_2 coated sand grains could be regarded as Y zeolite. BET results corroborate the images of Figure 1, in which one can verify smoother sand grain surface before any treatment, with a significant roughness achieved after TiO_2 layer formation. Further, these results indicate that the synthetic procedure builds an amorphous material with high surface area, an important characteristic for catalysts, leading to higher reaction rates. XRD data are on the SI section (Figures S6-S9).

Table 2. BET data for water washed sand, sand supported catalyst and Evonik's Aerolyst 7711

Sample	Specific surface area / ($m^2\ g^{-1}$)	Pore volume / ($cm^3\ g^{-1}$)
Sand grains	0.8	5.9×10^{-4}
Sand@TiO_2	296.4	9.9×10^{-2}
Aerolyst 7711	52.0	2.8×10^{-1}

MB degradation was followed by UV-Vis spectroscopy. 3 g of sand@TiO_2 was left in contact with the 20 mL aqueous solution of MB at 3×10^{-5} mol L^{-1} for 30 min prior to irradiation (sand@TiO_2 UV-Vis spectra in Figure S10, SI section). Under dark conditions, sand@TiO_2 removed almost 20% of the MB. In the presence of light UV all MB absorption bands continuously decreased (ca. 70%) for 7 min (Figure 3), and after 24 h of reaction, the total organic carbon (TOC) was ca. 5% of the initial mass. No reaction was obtained when sand grains were used without TiO_2 coating.

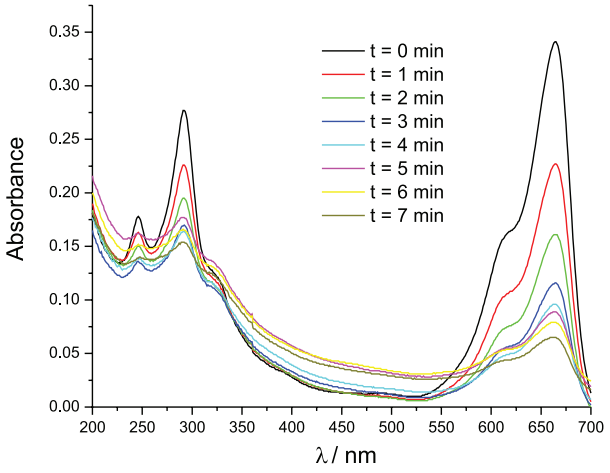

Figure 3. Absorption spectra for MB solution (10^{-4} mol L^{-1}) degradation under UV light.

On the other hand, for the Evonik TiO_2 the MB adsorption in dark conditions reached 45% and, after 7 min of irradiation, ca. 80% of the MB was photodegraded (using the same reaction conditions as for the sand@TiO_2 catalyst). Although a lower photodegradation was achieved by the sand@TiO_2 catalyst when compared to the Evonik's material, it is worthwhile to notice that the total catalyst masses are immensely different. While Evonik catalyst is 100% TiO_2 in mass, the sand@TiO_2 is less than 1% of the TiO_2 in weight on the sand grains surface.

The MB oxidation reactions on the TiO_2 surface (sand@TiO_2 or Evonik Aerolyst 7711 materials) is started by $OH^{\cdot}$ species. In a typical MB photodegradation study followed by high-performance liquid chromatography (HPLC) analysis, the authors[46] could propose the attack to the S atom in the central ring as the responsible for the solution discoloration, due to the loss of π-conjugation on MB electronic structure (Scheme 3). The reaction proceeds until the total destruction of the central ring. The resulting molecules go to CO_2 product by non-detectable intermediates.

Figure 4 shows the methylene blue degradation kinetics tracked at 664 nm. The best fit obtained by plotting ln (I/I_0) × irradiation time, indicated a reaction rate of 0.069 min^{-1} at 664 nm. It is worthwhile to observed that the same reaction rate was obtained when the same catalyst sample was submitted twice to new MB solutions at the same MB concentration (2nd and 3rd runs, Figure 4). These results indicate that the TiO_2 coating was not washed out of the sand surface. Although simplistic, this experiment shows that the sand@TiO_2 catalyst is a promising material for photochemical treatment with enhanced performance. Recent related publications[34-36] are not comparable to the one showed here, because, in average, they are expensive due to the necessity of employing noble metals or

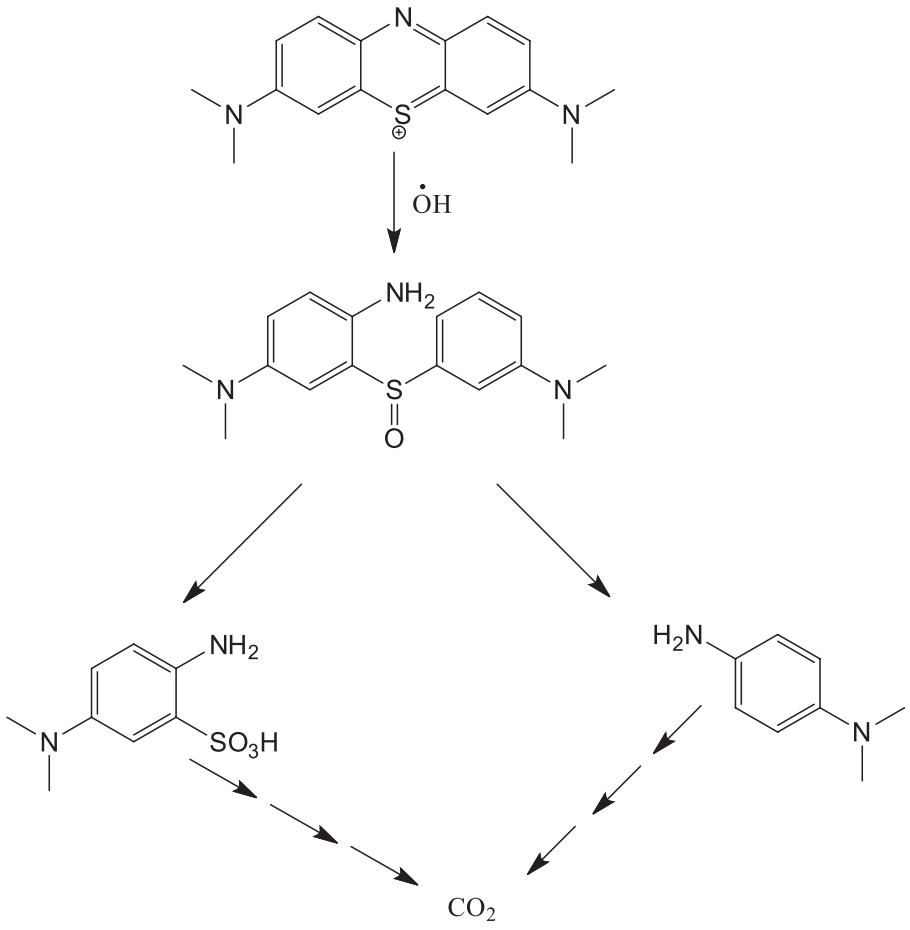

Scheme 3. MB degradation over TiO_2 surface.[46]

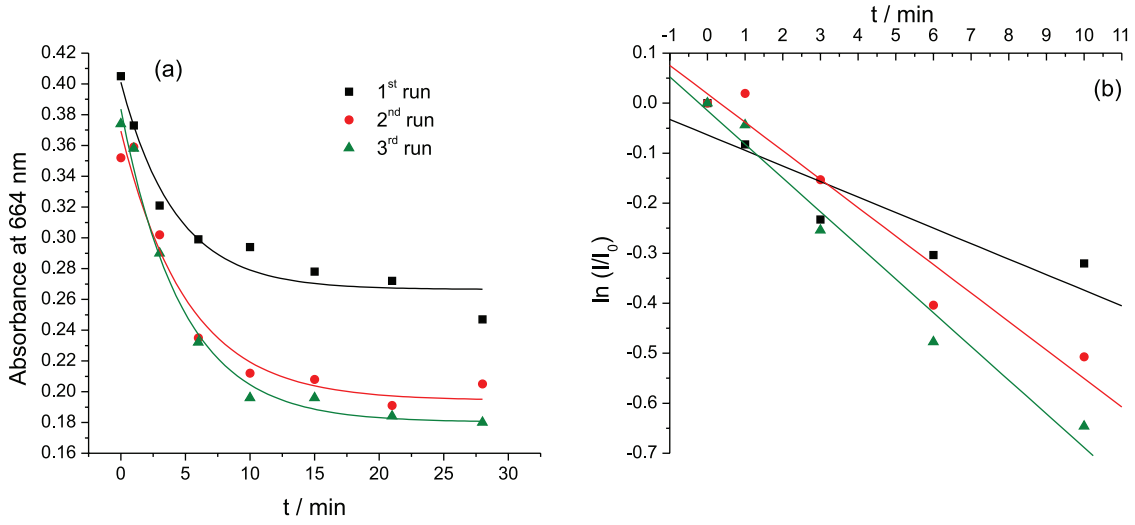

Figure 4. (a) Absorbance decay for degradation tests and (b) respective ln $(I/I_0) \times t$ linear fit at 664 nm.

nano-dimension. Nevertheless, both problems are obstacles to the widespread use of the photocatalysis technology for water treatment.

It is also important to notice that the almost complete MB bleaching was achieved in 7 min by 3 g of sand@TiO_2. This result can be assigned to a competition mechanism for the MB consumption, where the dye is directly consumed by the intermediate reaction between TiO_2 and H_2O or O_2 (path A, Figure 5) or by the electronically excited dye oxidation over the catalyst (path B, Figure 5).

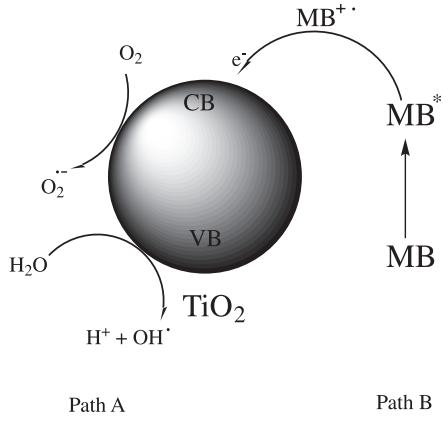

Figure 5. Methylene blue photodegradation reactions.

In path A the UV photons excite TiO_2 electrons from the valence band (generating holes, h^+) to the conduction band (generating electrons, e^-), originating electron-hole pairs. The valence band holes and conduction band electrons can migrate to the TiO_2 surface and, then, react with H_2O and O_2, respectively. In path B the electronically excited MB can donate one electron to the TiO_2 valence band, giving rise to $MB^{+\bullet}$.

To confirm the MB photodegradation on path B mechanism, the photodegradation experiment was repeated by using pyrex reactor covered with a long pass red filter in order to avoid light absorption by the sand@TiO_2 system.

As expected, when MB is the only excited component on the reaction medium the photodegradation reaction rate decreases (0.047 L mol min^{-1}) ca. 30% when compared to the one without longer pass filter (0.069 L mol min^{-1}, where both sand@TiO_2 and MB absorb light).

As the interest in flow reactions has increased both on academia and on industries, the MB photodegradation was evaluated using a simple flow reactor. The advantage of such reactors is directly related to the reduction of reaction time and reactor size, as well as by enhancing light absorption by the photocatalyst due to the thin water layer over it. Figure 6 shows MB photodegradation under flow conditions (recirculating). Under recirculation conditions (110 mL min^{-1}), three treatment cycles (total of 120 min) were necessary to reduce absorbance at 664 nm in 90%.

The photodegradation of ciprofloxacin was evaluated in water (13 mg in 20 mL, pH = 7.0) and 3 g of the sand@TiO_2 using a beaker as a steady state reactor. As can be seen on Figure 7, the antibiotic was almost completely degraded in 20 min and the reaction rate for ciprofloxacin was 0.061 min^{-1}, almost the same found when MB was used as a probe regardless the different chemical structures. After 24 h of reaction, the total organic carbon was ca. 3% of the initial mass. Differently from MB, the antibiotic is slowly photodegraded by UV irradiation with a reaction rate of 0.004 min^{-1} (using the same method but without sand@TiO_2 catalyst). No other absorption band is recognizable during the antibiotic degradation. Under flow reaction CIP was photodegraded in 120 min (Figure S11, SI section). No reaction occurred when sand grains were used without TiO_2 coating. As CIP shows UV-Vis absorption spectrum in the same region of TiO_2 it is expected that paths A and B mechanisms are operating during the photodegradation course.

Lastly, an actual non-treated wastewater sample from a cloth's dyeing company (DeMillus) was tested in a batch experiment using our sand@TiO_2 catalyst. The sample was diluted with distilled water without further purification. As can be seen in Figure 8 the reaction promoted significant water coloration decrease after 24 h of irradiation. The TOC analysis gave a total reduction of dissolved organic matter

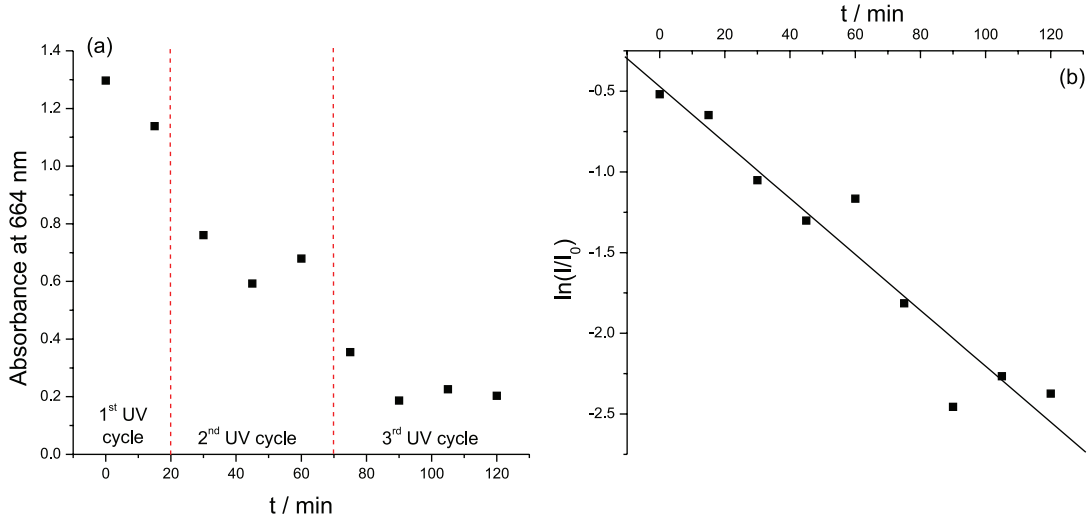

Figure 6. (a) Absorbance decay for methylene blue degradation tests with recirculation and (b) respective ln $(I/I_0) \times t$ linear fit at 664 nm.

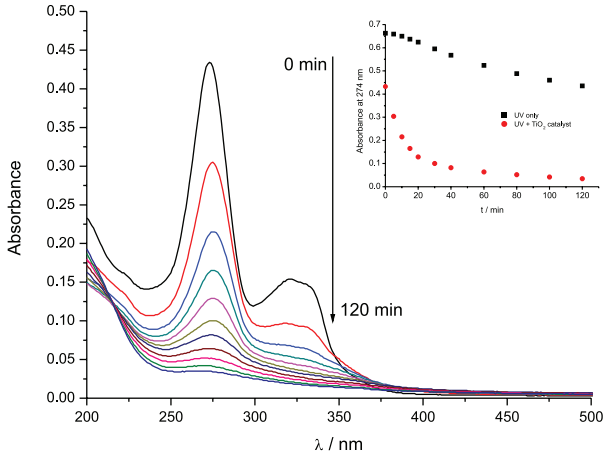

Figure 7. Ciprofloxacin photodegradation over sand@TiO_2 catalyst.

close to 90%. Although not being a definitive test, result shows that sand@TiO_2 catalyst is a promising alternative for contaminated water treating.

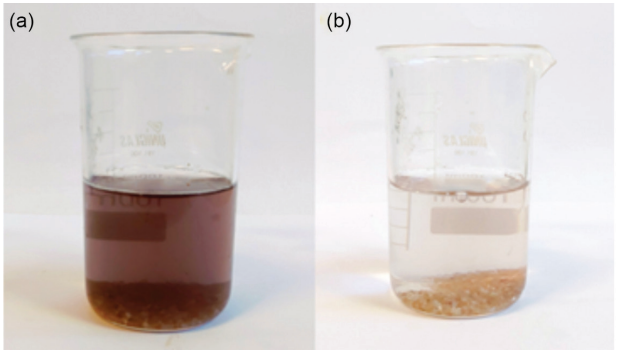

Figure 8. Pictures of wastewater (a) before and (b) after photodegradation.

Conclusions

A new non-expensive catalyst was obtained by covalent bonding of TiO_2 to sand grains. FESEM/EDS images show a homogeneous dispersed TiO_2 coating over the sand grains surface. The results showed in the XPS spectra of sand@TiO_2 samples indicate the successful chemical modification of the silica sand grains. This material was evaluated as photocatalyst by employing MB as a probe and a real sample from dyeing cloth industry. Both tests showed that the sand@TiO_2 material is a promising catalyst for photodegradation of dyes in water. Additionally, the photocatalyst showed as an efficient solution for treating ciprofloxacin contaminated water. The results indicate that the synthesized catalyst has great application potential in water and wastewater treatment reactors, mainly due to its thin TiO_2 layer chemically bonded to an inert and low-cost support in photocatalytic oxidation.

Supplementary Information

Supplementary information is available free of charge at http://jbcs.sbq.org.br as PDF file.

Acknowledgments

Authors thank to CNPq and CAPES for funding and DeMillus for wastewater sample.

References

1. Anastas, P.; Eghbali, N.; *Chem. Soc. Rev.* **2010**, *39*, 301.
2. Kralisch, D.; Ott, D.; Gericke, D.; *Green Chem.* **2015**, *17*, 123.
3. Ravelli, D.; Fagnoni, M.; Dondi, D.; Albini, A.; *J. Adv. Oxid. Technol.* **2011**, *14*, 5.
4. Tichá, M.; Žilka, M.; Stieberová, B.; Freiberg, F.; *Integr. Environ. Assess. Manage*. **2016**, *12*, 478.
5. Zhou, Q.; Fang, Z.; Li, J.; Wang, M.; *Microporous Mesoporous Mater.* **2015**, *202*, 22.
6. Turiel, E.; Bordin, G.; Rodriguez, A. R.; *J. Environ. Monit.* **2005**, *7*, 189.
7. Dantas, G.; Sommer, M. O.; Oluwasegun, R. D.; Church, G. M.; *Science* **2008**, *320*, 100.
8. U.S. Food and Drug Administration (FDA); *Cipro Label, Reference ID: 3985477*; FDA, 2016. Available at https://www.accessdata.fda.gov/drugsatfda_docs/label/2016/019537s085,020780s042lbl.pdf, accessed in May 2019.
9. Tsui, W. H.; Yim, G.; Wang, H. H.; McClure, J. E.; Surette, M. G.; Davies, J.; *Chem. Biol.* **2004**, *11*, 1307.
10. Linares, J. F.; Gustafsson, I.; Baquero, F.; Martinez, J. L.; *Proc. Natl. Acad. Sci. U. S. A.* **2006**, *103*, 19484.
11. Linares, J. F.; Lopez, J. A.; Camafeita, E.; Albar, J. P.; Rojo, F.; Martinez, J. L.; *J. Bacteriol.* **2005**, *187*, 1384.
12. Li, C.; Xu, Y.; Tu, W.; Chen, G.; Xu, R.; *Green Chem.* **2017**, *19*, 882.
13. Carmosini, N.; Lee, L. S.; *Chemosphere* **2009**, *77*, 813.
14. Turchi, C.; *J. Catal.* **1990**, *122*, 178.
15. Li, C.; Chen, G.; Sun, J.; Feng, Y.; Dong, H.; Han, Z.; Hu, Y.; Lv, C.; *New J. Chem.* **2015**, *39*, 4384.
16. Dong, F.; Li, Y.; Wang, Z.; Ho, W.-K.; *Appl. Surf. Sci.* **2015**, *358*, 393.
17. Lu, Z.; Zhu, Z.; Wang, D.; Ma, Z.; Shi, W.; Yan, Y.; Zhao, X.; Dong, H.; Yang, L.; Hua, Z.; *Catal. Sci. Technol.* **2016**, *6*, 1367.
18. Wang, P.; Tang, Y.; Dong, Z.; Chen, Z.; Lim, T. T.; *J. Mater. Chem. A* **2013**, *1*, 4718.
19. Fujishima, A.; Honda, K.; *Nature* **1972**, *238*, 37.
20. Nakata, K.; Fujishima, A.; *J. Photochem. Photobiol., C* **2012**, *13*, 169.
21. Fujishima, A.; Zhang, X.; Tryk, D. A.; *Int. J. Hydrogen Energy* **2007**, *32*, 2664.

22. Makama, A. B.; Salmiaton, A.; Saion, E. B.; Choong, T. Y.; Abdullah, N.; *Int. J. Photoenergy* **2016**, *2016*, DOI: 10.1155/2016/2947510.
23. Grabowska, E.; Reszczynska, J.; Zaleska, A.; *Water Res.* **2012**, *46*, 5471.
24. Jiang, Z.; Zhu, C.; Wan, W.; Qian, K.; Xie, J.; *J. Mater. Chem. A* **2016**, *4*, 1806.
25. Hendrix, Y.; Lazaro, A.; Yu, Q.; Brouwers, J.; *World J. Nano Sci. Eng.* **2015**, *5*, 161.
26. Xuzuang, Y.; Yang, D.; Huaiyong, Z.; Jiangwen, L.; Martins, W. N.; Frost, R.; Daniels, L.; Yuenian, S.; *J. Phys. Chem. C* **2009**, *113*, 8243.
27. da Rocha, O. R. S.; Dantas, R. F.; Duarte, M. M. M. B.; Duarte, M. M. L.; da Silva, V. L.; *Chem. Eng. J.* **2010**, *157*, 80.
28. Chong, M. N.; Jin, B.; Chow, C. W.; Saint, C.; *Water Res.* **2010**, *44*, 2997.
29. Pirovano, C.; Guidotti, M.; Dal Santo, V.; Psaro, R.; Koldeeva, O. A.; Ivanchikova, I. D.; *Catal. Today* **2012**, *197*, 170.
30. Anpo, M.; Takeuchi, M.; *J. Catal*. **2003**, *216*, 505.
31. Dietrich, L. A.; Sahu, M.; Biswas, P.; Fein, J. B.; *Chem. Geol.* **2012**, *332-333*, 148.
32. Serrano, D. P.; Calleja, G.; Sanz, R.; Pizarro, P.; *J. Mater. Chem.* **2007**, *17*, 1178.
33. Bai, X.; Zhang, X.; Hua, Z.; Ma, W.; Dai, Z.; Huang, X.; Gu, H.; *J. Alloys Compd.* **2014**, *599*, 10.
34. Li, W.; Bak, T.; Atanacio, A.; Nowotny, J.; *Appl. Catal., B* **2016**, *198*, 243.
35. Li, X.; Yu, J.; Low, J.; Fang, Y.; Xiao, J.; Chen, X.; *J. Mater. Chem. A* **2015**, *3*, 2485.
36. Górska, P.; Zaleska, A.; Kowalska, E.; Klimczuk, T.; Sobczak, J. W.; Skwarek, E.; Janusz, W.; Hupka, J.; *Appl. Catal., B* **2008**, *84*, 440.
37. Zhu, H.; Goswami, N.; Yao, Q.; Chen, T.; Liu, Y.; Xu, Q.; Chen, D.; Lu, J.; Xie, J.; *J. Mater. Chem. A* **2018**, *6*, 1102.
38. Luo, L.; Cooper, A. T.; Fan, M.; *J. Hazard. Mater.* **2009**, *161*, 175.
39. Lee, S. Y.; Park, S. J.; *J. Ind. Eng. Chem.* **2013**, *19*, 1761.
40. Kanakaraju, D.; Glass, B. D.; Oelgemöller, M.; *Environ. Chem. Lett.* **2014**, *12*, 27.
41. Giovannetti, R.; D'Amato, C. A.; Zannotti, M.; Rommozzi, E.; Gunnella, R.; Minicucci, M.; Di Cicco, A.; *Sci. Rep.* **2015**, *5*, 17801.
42. Erdem, B.; Hunsicker, R. A.; Simmons, G. W.; Sudol, E. D.; Dimonie, V. L.; El-Aasser, M. S.; *Langmuir* **2001**, *17*, 2664.
43. Hanaor, D. A. H.; Sorrell, C. C.; *Adv. Eng. Mater.* **2014**, *16*, 248; Abdel-Maksoud, Y. K.; Imam, E.; Ramadan, A. R.; *Catal. Today* **2018**, *313*, 55.
44. Yousheng, T.; Hirofumi, K.; Katsumi, K.; *J. Phys. Chem. B* **2003**, *107*, 10974.
45. Nosaka, Y.; Nosaka, A. Y.; *Chem. Rev.* **2017**, *117*, 11302; Liao, H.; Reitberger, T.; *Catalysts* **2013**, *3*, 418; Hurum, D. C.; Agrios, A. G.; Gray, K. A.; Rajh, T.; Thurnauer, M. C.; *J. Phys. Chem. B* **2003**, *107*, 4545.
46. Zuo, R.; Du, G.; Zhang, W.; Liu, L.; Liu, Y.; Mei, L.; Li, Z.; *Adv. Mat. Sci. Eng.* **2014**, *2014*, DOI: 10.1155/2014/170148.

Submitted: December 28, 2018
Published online: June 6, 2019